In Situ Electrochemical Investigation of Acidic Pressure Oxidation of Pyrite at 160–240°C

Can Cui,[1] Heping Li, [1,z] Sen Lin,[1] and Pan Wang[1,2]

[1]*Key Laboratory of High-temperature and High-pressure Study of the Earth's Interior, Institute of Geochemistry, Chinese Academy of Sciences, Guiyang 550002, People's Republic of China*
[2]*University of Chinese Academy of Sciences, Beijing, 100049, People's Republic of China*

In situ electrochemical studies on the oxidation behavior of pyrite in 0.1 M H_2SO_4 solution in the temperature range of 160 to 240°C were performed by measurements of electrochemical impedance spectroscopy (EIS), linear polarization, potentiodynamic polarization and potentiostatic polarization. Results showed that with the increase of temperature, the anodic current density increased, while the corrosion potential (E_{corr}), polarization resistance, charge transfer resistance (R_{ct}) and pore resistance (R_{pore}) decreased. The change of these electrochemical parameters indicated that the increase of temperature promoted the dissolution of pyrite by accelerating the electrochemical step and weakening of the porous passive film. EIS studies with different applied potentials at 240°C revealed that both R_{ct} and R_{pore} decreased with increasing applied potential. As the potential increased to 400 mV, the time constant relating to the porous passive film disappeared. These changes demonstrated that sulfur yield was dependent on the potential, and the sulfur yield approached zero at 400 mV at the temperature of 240°C. The values of E_a indicated that pyrite oxidation kinetics were limited by the rate of electrochemical reaction.

With large-scale gold mining, rich deposits are increasingly exhausted, and low grade and refractory deposits will become the main resources of the gold industry.[1–4] Pyrite is an important gold bearing refractory ore, and microscopic and ultramicroscopic gold particles are finely dispersed in the lattice of pyrite.[5–7] The encapsulation of pyrite results in poor gold recovery with conventional cyanide-leaching process, even when the ore is finely ground. In order to enhance the release of gold particles and render the gold accessible to cyanide and oxygen, pressure oxidation of refractory gold ores is often carried out as an essential pretreatment step prior to cyanidation.[8–11] In the pressure oxidation process, gold bearing pyrite is subjected to high-temperature, high-pressure oxidation in autoclaves to destroy pyrite lattice.[12,13] This process has been practiced commercially since the early1980s,[14] and is widely accepted by the gold mining industry all over the world for its high efficiency and low pollution.

Pressure oxidation of pyrite has been extensively investigated in recent decades.[15,16] Previous researchers have found that the chemistry of oxidative leaching is complicated due to the heterogeneous nature of pyrite, and there has been much debate about the various leaching mechanisms involved. However, there is a general agreement that the dissolution reaction proceeds via an electrochemical reaction mechanism.[17–19] In most of the pressure oxidation experiments reported, the oxidation of pyrite was found to yield ferric sulfate, ferrous sulfate, elemental sulfur or sulfuric acid with various temperatures, acidities and oxygen partial pressures.[20,21] King and Lewis[22] found that the increase of temperature (80–100°C) positively affected pyrite dissolution, and a 90% conversion was achieved in 4 h at 100°C with 120 psig O_2, 0.5 M Fe^{3+} and 20 g/L pyrite loading. Beily and Peters[23] investigated the pressure oxidation of pyrite in 0.01–3 M H_2SO_4 solution at 85–130°C. The dissolution mechanism was found to be electrochemical and was a potentiostatically controlled steady state between sulfate-forming and elemental sulfur-forming anodic reactions:

$$FeS_2 + 8H_2O \rightarrow Fe^{2+} + 2SO_4{}^{2-} + 16H^+ + 14e^- \qquad [1]$$

$$FeS_2 \rightarrow Fe^{2+} + 2S + 2e^- \qquad [2]$$
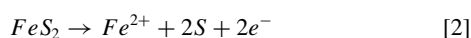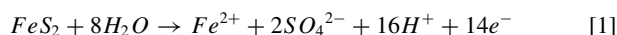
They also claimed that a layer of liquid sulfur film was formed on the pyrite surface at temperatures above 119°C, and thus inhibited the pyrite dissolution. Papangelakis and Demopoulos[24] pointed out that

the oxidation kinetics of pyrite at 140–180°C followed a shrinking core model, with the surface chemical reaction as the rate-controlling step, and the reaction proceeded to completion only at temperatures exceeding 160°C. Long and Dixon[25] studied the pressure oxidation kinetics of pyrite in sulfuric acid media at 170–230°C. They proposed a new "passivating shrinking sphere" model which fitted the conversion data more precisely over the entire temperature range, and established that increasing temperature had a significant influence on the rate of dissolution, with nearly all the pyrite dissolved at 230°C within 20 min. Zhukov et al.[26] developed a comprehensive kinetic model for aqueous-phase oxidation of pyrite using novel Markov chain Monte Carlo (MCMC) methods, the results showed that pyrite surface reactions with both molecular oxygen and ferric ions were important at the studied experimental conditions, and their relative importance depended on the pyrite slurry concentration.

Pressure oxidation of pyrite was usually studied using conventional solution chemistry,[27–29] spectroscopic[30,31] and other ex situ techniques.[32] These ex situ methods have their advantages, but their drawbacks cannot be ignored. Firstly, in the process of cooling and unloading, the existing states and concentrations of components in electrolyte solution may change, and a secondary mineral may be formed on the pyrite surface. Secondly, the solid-liquid interface information has important significance to study the reaction mechanism, but the traditional ex situ research methods are unable to achieve this goal. To resolve these issues, it is urgent to develop in situ research techniques. As we know that electrochemical methods are effective in situ research tools for study of the redox reactions, and have been widely used in the research on the oxidation process of pyrite at lower temperatures.[33–35] Considering that pressure oxidation of pyrite is an electrochemical process, investigation of oxidative dissolution of pyrite at high temperatures using in situ electrochemical techniques is feasible. Little has been published on pyrite dissolution in the temperature range of 160 to 240°C using in situ electrochemical methods, probably because of the technical difficulties. Investigation of oxidation behavior of pyrite at such hydrothermal environments using in situ electrochemical techniques may be helpful to understand the process of pyrite pressure oxidation from the perspective of electrochemistry.

The present work studied the electrochemical behavior of pyrite acid pressure oxidation over the temperature range from 160 to 240°C, which is the range employed by most commercial plants.[25] All experiments were performed in an autoclave with three electrodes. The influence of temperature and applied potential on the oxidation behavior of pyrite was investigated by the measurements of electrochemical
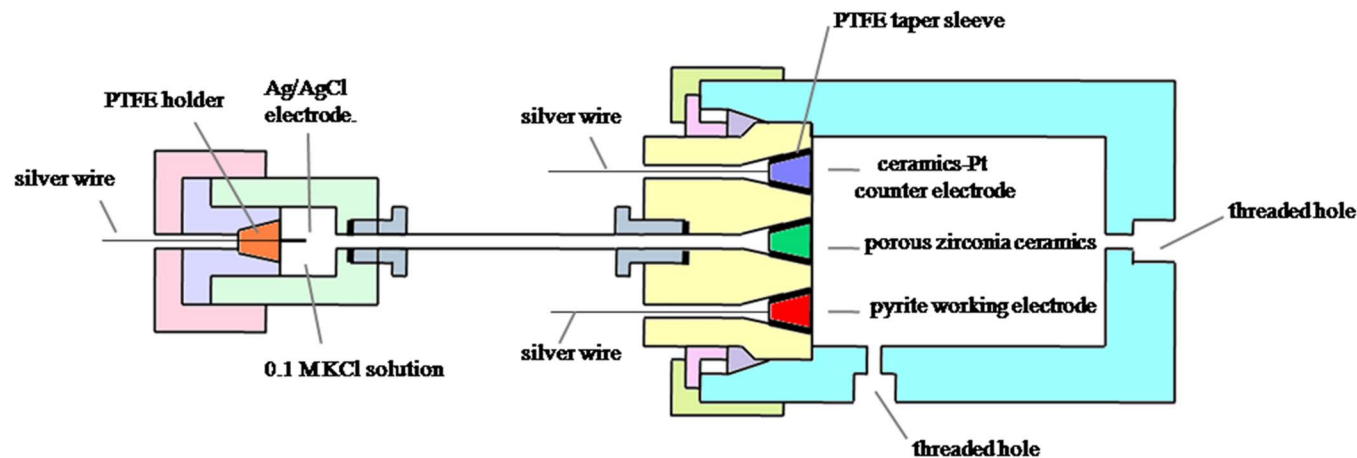
[z]E-mail: liheping@vip.gyig.ac.cn

Figure 1. Schematic of the autoclave electrochemical measurements system.

impedance spectroscopy (EIS), linear polarization plots, potentiodynamic polarization and potentiostatic polarization curves.

Experimental

Materials and apparatus.—All experiments were performed in a titanium alloy autoclave with three electrodes, schematic of the apparatus is shown in Figure 1. The pyrite sample came from Zhaoyuan, Shandong, China. The pyrite crystal structure was confirmed by X-ray diffraction. Electron microprobe analysis confirmed that Fe and S contents (in wt%) of the pyrite sample were 46.53 and 51.66%, respectively. The main impurity was SiO_2, but the influence of SiO_2 on the electrochemical behavior of the surface is not significant. Furthermore, trace impurity elements were found, including Cu (308 pmm), Ni (251 ppm) and Co (49.8 ppm). The test solution was sulfuric acid solution prepared with ultrapure water and analytical grade chemical reagent with the concentration of 0.1 M.

The pyrite working electrode was obtained by cutting bulk pyrite by a lathe into a cone frustum with a working area of 0.28 cm^2. The pyrite electrode was sealed and electrically insulated from the autoclave plug with a 1 mm thick PTFE taper sleeve, which was obtained from machining a PTFE bar (Daikin Fluorochemicals (China) Co., Ltd.). The PTFE taper sleeve together with pyrite electrode cone frustum were inserted into the tapered bore at the autoclave plug with the aid of a hydraulic press machine. The working electrode cone frustum, PTFE taper sleeve, and the tapered bore at the autoclave plug make up a conical self-energizing sealing structure. Electrical connection was made with a silver wire held at the smaller end plane of the working electrode with high temperature resistant conductive adhesive, and an alumina ceramics tube was utilized to insulate the silver wire from the autoclave plug. The counter electrode was a self-made alumina ceramic cone frustum with a platinum wire inside, and platinum powder was sintered on the round surface of the ceramic to achieve sufficient counter electrode surface area. The assembling manner of the counter electrode was the same as the working electrode. The reference electrode was an external pressure-balanced Ag/AgCl electrode, which was filled with 0.1 M KCl solution, and a porous zirconia ceramics (also sealed by PTFE taper sleeve) was used to separate the experimental and reference solution. All potentials mentioned in this work are normalized with respect to the saturated hydrogen electrode (SHE) using the following formula.[36]

$$\Delta E_{SHE} = \Delta E_{obs} + 286.6 - \Delta T + 1.745 \times 10^{-4} \Delta T^2$$
$$- 3.03 \times 10^{-6} \Delta T^3 (mV) \quad [3]$$

Electrochemical measurements.—Before each electrochemical experiment, the working electrode was mechanically ground using

a series of silicon carbide (SiC) grit papers up to grade 5000 and cleaned with acetone and distilled water. To avoid the oxidation of pyrite when heated, high purified argon gas was introduced into the autoclave to drive the air out before heating. After the autoclave was heated to the set temperature, 20 mL of 0.1 M sulfuric acid solution was pumped into the autoclave using a pressure pump. The sulfuric acid solution was deoxidized by bubbling purified argon gas before injection, to eliminate the effect of dissolved oxygen, and the concentration of dissolved oxygen was approximately 0.13 ppm. Electrochemical measurements were carried out by using a Princeton Applied Research (PAR) 2263 electrochemical workstation along with Powersuite software. The open circuit potential (OCP) was carefully observed after immersing the working electrode in the test solution until the potential stabilized within ± 2 mV. Once the potential stability was established, an EIS test was initialed and recorded. The scanning frequency was selected in the range of 10 kHz - 100 mHz, and the AC amplitude was 10 mV. Software ZSimpWin (Version 3.10) was employed to fit the EIS data. Afterwards, linear polarization curves were obtained by scanning in the forward direction from −10 mV vs. OCP to 10 mV vs. OCP at a scan rate of 0.166 mV/s, and the potentiodynamic polarization plots were measured by scanning in the forward direction from −150 mV vs. OCP to 300 mV vs. OCP at a scan rate of 1 mV/s. Potentiostatic polarization measurements were taken at the specific potentials of 200 and 400 mV vs. SHE, and the current densities were recorded 3 min after onset of the measurements, when the current densities became relatively stabilized. For each experimental condition, three measurements were performed to ensure the reliability and reproducibility of the data.

Results and Discussion

EIS measurements at different temperatures.—EIS has been normally used to study the oxidation behavior and passivation phenomena for different metals and ores in a variety of environments.[37,38] In the present research, the effect of temperature on electrochemical oxidation behavior of pyrite was studied in 0.1 M H_2SO_4 solution at different temperatures of 160, 180, 200, 220, and 240°C with saturated vapor pressure, Bode plots obtained at OCP are shown in Figure 2. The impedance of the interface (|Z|) showed low values at high frequency, it increased quickly with decreasing frequency in low frequency region, and the highest value of |Z| was recorded at the lowest frequency. In addition, increasing the temperature was obvious to decrease the values of |Z|, especially at low frequency. The result indicates that the increase of temperature accelerates the dissolution of pyrite. According to Bode phase plots at different temperatures, two time constants were observed. The time constant at lower frequency is related to the double layer and the one at higher frequency is attributed to the presence of porous passive film at the pyrite surface.
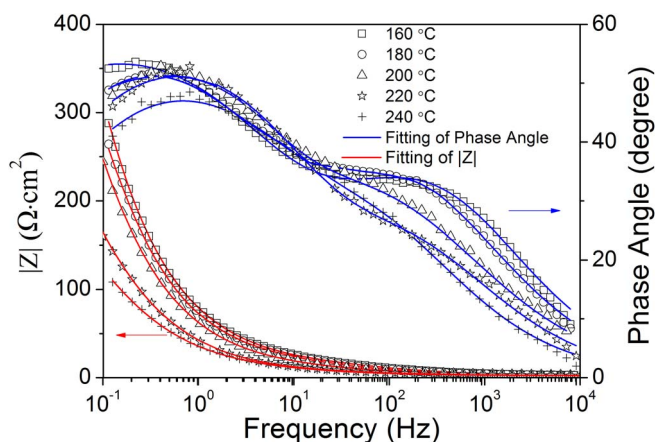
Figure 2. Bode plots for pyrite at OCP in 0.1 M sulfuric acid solution at different temperatures.

Figure 4. Potentiodynamic polarization plots for pyrite in 0.1 M sulfuric acid solution at different temperatures, with a scan rate of 1 mV/s.
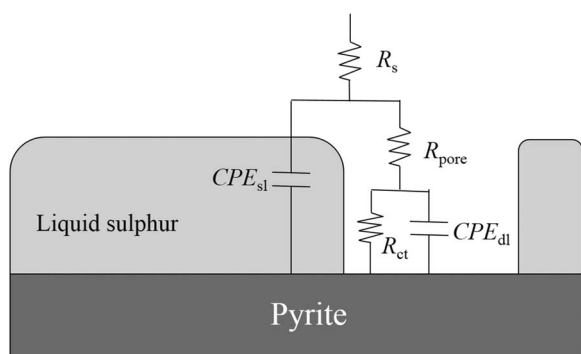

Figure 3. Equivalent circuit for pyrite in 0.1 M sulfuric acid solution at different temperatures.

Oxidation of pyrite is a non-uniform corrosion process, oxidant attacks on pyrite surface preferentially at sites of defects and imperfections which have smaller bandgap and higher dangling bond densities, the charge transfer rate at these sites are much faster compared to sites with normal coordination.[21] Thus, elemental sulfur that formed as a result of Reaction 2 is accumulated mainly around these sites. The studied temperature range (160–240°C) is above the melting point of sulfur (119°C), thus elemental sulfur exists in the form of liquid, and it exhibits very high viscosity and poor mobility due to its chain structure.[24] The accumulation of such liquid sulfur around the active sites leads to partial coverage of the pyrite surface. Thus, the liquid sulfur layer can be considered as a porous passive film.[23–25] The coverage of this porous film not only causes a decrease in exposed electrode area, but also increases the resistance of mass transfer process. Therefore, the equivalent circuit shown in Figure 3 was used to fit the experimental results, where CPE_{dl} represents the double layer capacitance, CPE_{sl} is the capacitance of the surface layer, R_s and R_{pore} correspond to the solution resistance and the pore resistance, respectively. R_{ct} represents the charge transfer resistance. A constant phase
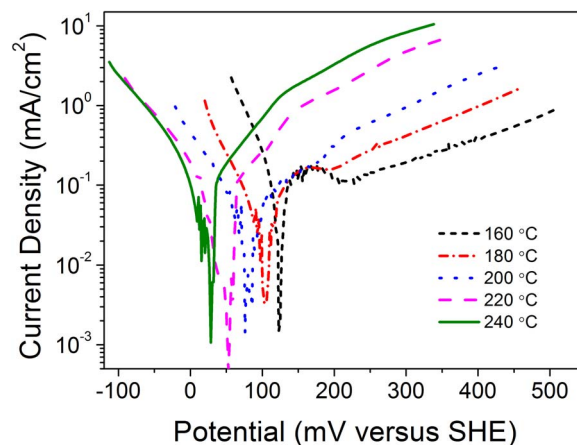
element (CPE) is used to replace pure capacitance (C) due to the surface roughness and nonuniformity of pyrite electrode, as reported previously.[39] The values of these parameters are illustrated in Table I.

R_{ct} is a characteristic quantity for the charge transfer step of an electrode electrochemical reaction which usually reflects its inherent speed.[40] In this study, the value of R_{ct} decreased significantly with the increase in temperature. Specifically, when the temperature increased from 160 to 240°C, the value of R_{ct} decreased from 2480 to 382 $\Omega \cdot cm$,[2] suggesting that the oxidation rate increased. The value of R_{pore} is influenced by the porous liquid sulfur film at the pyrite surface. As seen, the value of R_{pore} decreased with the increasing temperature. This may be attributed to the fact that liquid sulfur diffuses into the solution more quickly at higher temperatures, and thus less sulfur accumulates on the pyrite surface, which leads to the decrease in liquid sulfur film thickness and the fraction of surface coverage. In other words, increasing temperature results in an increase in pore diameter and a decrease in pore depth, and thus the value of R_{pore} decreased from 27.9 to 5.37$\Omega \cdot cm^2$ when the temperature increased from 160 to 240°C. It is also noted that the value of R_{ct} is much higher than R_{pore} in the studied temperature range, indicating that the rate determining step of the reaction is the charge transfer step across the double layer.

Potentiodynamic polarization measurements at different temperatures.—In order to further investigate the effect of raising temperature on the oxidation behavior and passivation phenomena of pyrite in sulfuric acid solution, potentiodynamic polarization measurements were carried out. The polarization curves obtained for pyrite in 0.1 M H_2SO_4 solution at 160, 180, 200, 220, and 240°C, respectively with saturated vapor pressure are displayed in Figure 4. Increase of temperature was found to increase the anodic current density, while shift the corrosion potential to the more negative direction.

At the temperature of 160°C, the anodic current density increased rapidly when the potential was swept from the corrosion potential to 150 mV. As Reaction 2 progressed, S^0 may be the main product in this potential range.[23,41] However, at potentials higher than 150 mV,

Table I. Equivalent circuit model parameters for pyrite in 0.1 M sulfuric acid at different temperatures.

| Temperature (°C)	R_s ($\Omega \cdot cm^2$)	CPE_{dl} Y_0 ($S \cdot s^n \cdot cm^{-2}$)	n	R_{ct} ($\Omega \cdot cm^2$)	CPE_{sl} Y_0 ($S \cdot s^n \cdot cm^{-2}$)	n	R_{pore} ($\Omega \cdot cm^2$)	X^2
160	2.48 ± 0.22	1.64E-3 ± 2.0E-4	0.68 ± 0.02	2480 ± 273	1.51E-3 ± 1.4E-4	0.62 ± 0.02	27.9 ± 1.7	4.58E-4
180	2.38 ± 0.31	8.79E-4 ± 1.3E-4	0.92 ± 0.01	1890 ± 292	3.60E-3 ± 2.3E-4	0.54 ± 0.03	14.5 ± 1.6	1.52E-3
200	2.51 ± 0.30	1.45E-3 ± 2.2E-4	0.72 ± 0.02	788 ± 63.4	9.07E-3 ± 1.1E-3	0.48 ± 0.01	12.6 ± 0.5	7.86E-4
220	2.40 ± 0.16	2.04E-3 ± 1.6E-4	0.67 ± 0.02	667 ± 85.7	3.24E-3 ± 2.0E-4	0.63 ± 0.02	7.16 ± 0.6	8.62E-4
240	2.36 ± 0.12	3.75E-3 ± 4.4E-4	0.79 ± 0.01	382 ± 25.1	7.60E-2 ± 6.1E-3	0.58 ± 0.02	5.37 ± 0.4	1.31E-3
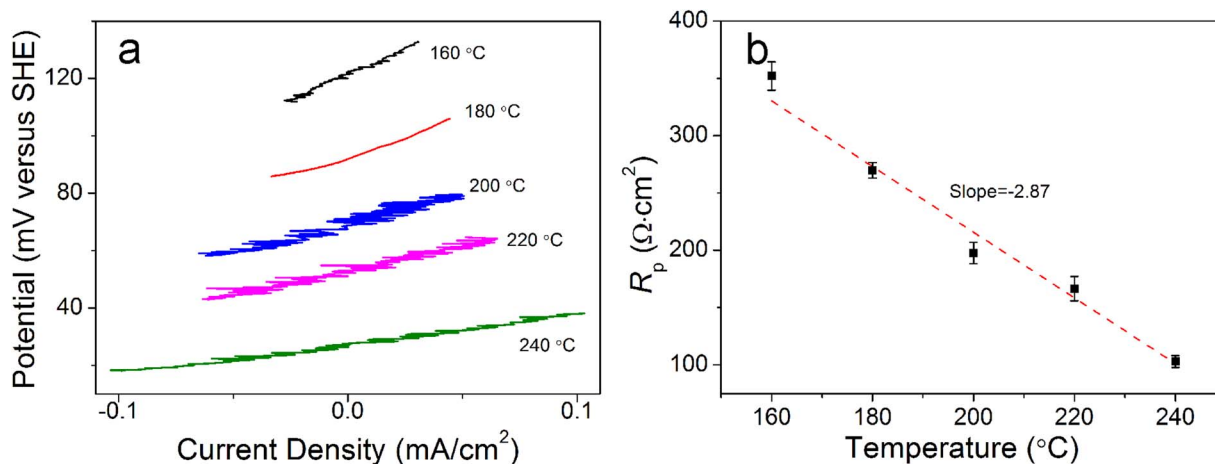
Figure 5. Linear polarization plots (a) and polarization resistance (R_p) (b) for pyrite in 0.1 M sulfuric acid solution at different temperatures, with a scan rate of 0.166 mV/s.

pyrite was transformed into the passivation region characterized by a decrease in the current density over a range of 150 to 210 mV. This may be due to the partly coating of pyrite by elemental sulfur formed by the previous dissolution of pyrite. The anodic current density once again increased with increasing potential at approximately 210 mV. This is mainly because of a rapid bulk dissolution process of pyrite (Reaction 1) above 210 mV,[23,42] and the previously formed elemental sulfur may be also oxidized to sulfate at high potentials, as described in Reaction 4.[43–45]

$$S^0 + 4H_2O \rightarrow SO_4^{2-} + 8H^+ + 6e^- \quad [4]$$
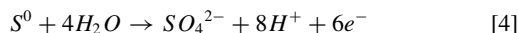
The phenomenon of passivation also appeared at the temperature of 180°C. Compared with the condition at 160°C, the decrease in current density was slighter, and the passivation region was narrower. At 200°C and higher temperatures, no decrease in current density could be observed. With the increase of temperature, the passivation phenomenon decreased gradually and eventually disappeared. This may be attributed to two reasons. Firstly, less elemental sulfur is formed at high temperatures.[23] Secondly, the increase in diffusion rate of liquid elemental sulfur with rising temperature results in less amount of elemental sulfur accumulates on pyrite surface. The potentiodynamic polarization data thus confirms the results obtained from the EIS measurements that the increase of temperature increases the dissolution of the investigated pyrite, also, it reveals that passivation phenomenon of pyrite electrode appears at 160 and 180°C and it decreases gradually with increasing temperature.

It is also noted that the cathodic current density decreases with increasing temperature. The cathodic process at pyrite surface is complex at the studied conditions, as three reactions may be involved. The first reaction is the reduction of oxygen, as described in Reaction 5.

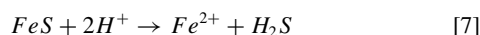$$1/2 O_2 + 2H^+ + 2e^- \rightarrow H_2O \quad [5]$$
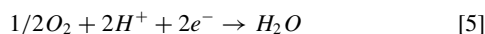
Though the experimental solution was deaerated by Ar bubbling, there was still residual dissolved oxygen, about 0.13 ppm measured by dissolved oxygen meter.

The second reaction is the reduction of pyrite, which can be represented by Reaction 6.[46]

$$FeS_2 + 2H^+ \rightarrow FeS + H_2S \quad [6]$$
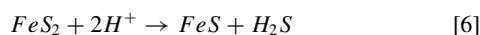
Then FeS dissolves in the acidic solution, as shown in Reaction 7.[47]

$$FeS + 2H^+ \rightarrow Fe^{2+} + H_2S \quad [7]$$

As shown in Figure 4, the corrosion potential of pyrite decreases with increasing temperature, which means that, at a constant cathodic potential, the overpotential for the reduction of pyrite decreases with increasing temperature.

The third reaction is the reduction of H$^+$. Pyrite and pyrite type compounds are considered as effective catalysts for hydrogen production.[48,49] H$^+$ can be reduced into H$_2$ at the pyrite surface, as described in Reaction 8.

$$2H^+ + 2e^- \rightarrow H_2 \quad [8]$$

The ionization constant of H$_2$SO$_4$ decreases with increasing temperature,[50] which causes a decrease in H$^+$ concentration. Thus, the H$^+$ reduction current density may decrease with increasing temperature.

The cathodic current density is related to the above three reduction reactions. Increasing temperature promotes the reduction of oxygen, however, it shows some negative effects on the reduction of pyrite and H$^+$. The decreasing cathodic current density with increasing temperature indicates that the reduction of pyrite and H$^+$ are the main reactions in the cathodic process.

The reduction products of pyrite and H$^+$ (Fe^{2+}, H$_2$S, H$_2$) may also be oxidized in the anodic polarization process, however, their diffusion coefficients are high at high temperatures, and they will diffuse into the solution quickly after they are generated. In this work, the potentiodynamic scanning was started from -150 mV vs. OCP, but not -250mV vs. OCP which is usually used in such studies, so the low cathodic overpotential decreased the production of these reduction products. Therefore, concentrations of these reduction products in the solution were quite limited, and their contribution to the anodic current density could be neglected.

Linear polarization measurements at different temperatures.—Figure 5a presents the linear polarization plots of pyrite in 0.1 M H$_2$SO$_4$ solution at 160, 180, 200, 220, and 240°C, respectively with saturated vapor pressure. The corrosion potential decreased with increasing temperature, which was in accordance with the potentiodynamic polarization plots. Polarization resistance (R_p) is an important parameter that reflects the oxidation behavior of pyrite. This is because that the value of R_p is inversely proportional to corrosion current density, and hence, a high value of R_p corresponds to a low dissolution rate. The R_p measured by the linear polarization curve is shown in Figure 5b. R_p decreased linearly with increasing temperature, and the slope was measured as -2.87 $\Omega \cdot$cm^2/°C, further indicating the dissolution of pyrite was positively affected by increasing temperature.

EIS measurements at different applied potentials.—In order to investigate the effect of applied potentials on the oxidation behavior and passivation phenomena of pyrite in sulfuric acid solution, the EIS measurements of pyrite were carried out in 0.1 M H$_2$SO$_4$ solution at 240°C with saturated vapor pressure. Bode plots obtained at potentials of OCP, 200 and 400 mV vs. SHE, respectively, are shown in
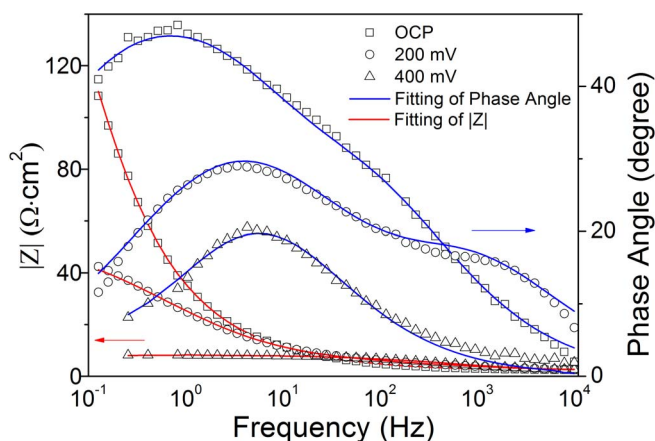
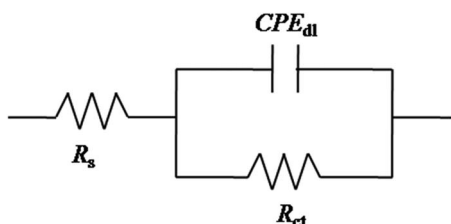**Figure 6.** Bode plots for pyrite in 0.1 M sulfuric acid solution at 240°C with different applied potentials.

Figure 7. Equivalent circuit for pyrite in 0.1 M sulfuric acid solution at 240°C with applied potential of 400 mV.

Figure 8. The Arrhenius plots for pyrite in 0.1 M sulfuric acid solution at different applied potentials.

Figure 6. The impedance of the interface ($|Z|$) showed lower values at high frequency, it increased with decreasing frequency obviously at OCP and 200 mV, however, it showed only a slight increase at 400 mV, from 2.6 to 8.0 $\Omega \cdot$ cm.[2] Furthermore, increasing the potential was obvious to decrease the values of $|Z|$, which indicates that pyrite dissolves more quickly at higher potentials. Bode phase plots revealed two time constants at OCP and 200 mV, which are related to the double layer and the porous passive film, respectively. While, only one time constant was observed at 400 mV, the time constant relating to porous passive film was absent. indicating that the liquid sulfur film at pyrite surface disappeared.

EIS data at OCP and 200 mV were analyzed by fitting the experimental results to the equivalent circuit shown in Figure 3, while, the equivalent circuit shown in Figure 7 was used to fit the data at 400 mV, fitting results are shown in Table II. The value of R_{ct} decreased significantly with the increase of applied potential. Specifically, when the potential increased from OCP to 400 mV, the value of R_{ct} decreased from 382 to 5.46 $\Omega \cdot$ cm,[2] suggesting the dissolution rate increased. Furthermore, the value of R_{pore} also decreased with increasing potential. This may be mainly attributed to the elemental sulfur yield decreases with rising potential,[23,51] indicating that the passivation phenomena of pyrite is mitigated at higher potential. It is important to notice that the time constant relating to the porous sulfur film disappears at 400 mV, which reveals that elemental sulfur yield for the anodic dissolution reaction tends to zero at 400 mV.
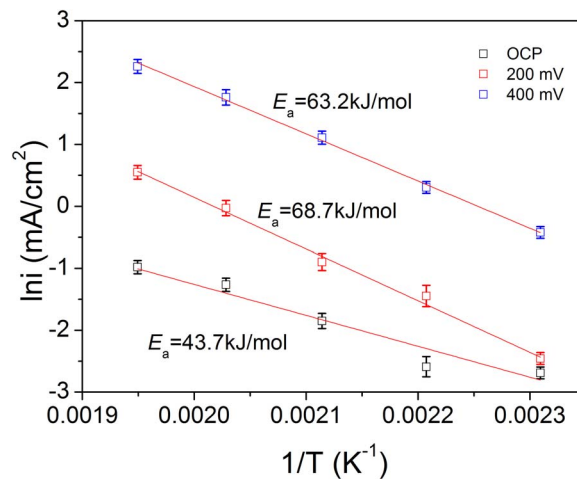
The dissolution of pyrite results in the formation of sulfur and sulfate as the final products, and the sulfur yield is dependent on the potential.[18,23,42,52] Flatt and Woods[42] indicated that sulfur yield approached zero at 1500 mV at the temperature of 26°C. This potential is the same as that found at 25°C by Biegler and Swift.[48] Bailey and Peters[23] found that at 1000 mV, essentially all the pyritic sulfur is reacting to produce sulfate by Reaction 1 at 110°C. In this study, the time constant associated with the porous sulfur film was present at OCP and 200 mV and disappeared at 400 mV, which demonstrates that the sulfate yield approaches 100% at 400 mV at the temperature of 240°C. The potential (400 mV) is lower than the values that reported at lower temperatures,[18,42,53] and it seems that the potential needed for 100% sulfate yield decreases with increasing temperature.

Potentiostatic polarization measurements.—Current densities for pyrite oxidation in 0.1 M sulfuric acid solution in the temperature range from 160 to 240°C at 200 and 400 mV vs. SHE were obtained by potentiostatic polarization measurements. The corrosion current densities at OCP were obtained from fitting of potentiodynamic polarization data. Apparent activation energy (E_a) can be calculated by the Arrhenius equation:

$$I = A \exp\left(\frac{-E_a}{RT}\right) \quad [9]$$

thus,

$$\ln I = \ln A - \frac{E_a}{RT} \quad [10]$$

finally,

$$E_a = -R \frac{d \ln I}{d\left(\frac{1}{T}\right)} \quad [11]$$

Figure 8 shows the Arrhenius plots for pyrite in 0.1 M sulfuric acid solution under different applied potentials, and values of E_a were obtained as 43.7, 68.7 and 63.2 kJ/mol, respectively at the potentials of OCP, 200 and 400 mV, over the temperature range 160–240°C.

Table II. Equivalent circuit model parameters for pyrite in 0.1 M sulfuric acid at 240°C with different applied potentials.

Applied potential (mV vs. SHE)	R_s ($\Omega \cdot$ cm^2)	CPE$_{dl}$ Y_0 (S$\cdot$s$^n \cdot$cm^{-2})	n	R_{ct} ($\Omega \cdot$ cm^2)	CPE$_{sl}$ Y_0 (S$\cdot$s$^n \cdot$cm^{-2})	n	R_{pore} ($\Omega \cdot$ cm^2)	X^2
OCP	2.36 ± 0.12	3.75E-3 ± 4.4 E-4	0.79 ± 0.01	382 ± 25.1	7.60E-2 ± 6.1 E-3	0.58 ± 0.02	5.37 ± 0.4	1.31E-3
200	2.46 ± 0.25	8.23E-3 ± 1.1 E-3	0.68 ± 0.02	46.2 ± 7.9	2.05E-3 ± 1.6 E-4	0.66 ± 0.03	3.08 ± 0.3	8.92E-4
400	2.51 ± 0.11	1.39E-3 ± 2.8 E-4	0.61 ± 0.02	5.46 ± 1.0	-	-	-	1.36E-3

Such values for the activation energy indicates that pyrite oxidation kinetics are limited by the rate of electrochemical reaction, and further demonstrates that temperature is a key factor for pyrite dissolution.

The value of 43.7 at OCP is close to most of the E_a values reported in the literature including the value of 41.7 kJ/mol reported by Long and Dixon[25] over the temperature range of 170–230°C, the value of 46.1 kJ/mol claimed by Zhukov[26] at 170–230°C, the E_a of 46.2 kJ/mol found in the paper of Papangelakis and Demopoulos[24] over the temperature range of 140–160°C, and the value of 51.1 kJ/mol reported by Beily and Peters[23] at 85–130°C. However, the E_a values at 200 and 400 mV in this study are higher than but not far from the previous reported values.

Conclusions

An investigation of electrochemical oxidation behavior of pyrite was carried out in 0.1 M H_2SO_4 solution at 160–240°C with different applied potentials. The influence of temperature and applied potential on the pressure oxidation of pyrite were investigated by EIS, linear polarization plots, potentiodynamic polarization and potentiostatic polarization curves. Several conclusions can be drawn from this research:

(1) The dissolution rate of pyrite increases with increasing temperature. The passivation phenomenon decreases gradually and eventually disappears with the increase of temperature.

(2) EIS studies at 240°C with applied potentials of OCP, 200 and 400 mV vs. SHE indicates that sulfate yield is dependent on the potential, and the sulfate yield approaches 100% at 400 mV at the temperature of 240°C. The potential (400 mV) is lower than the values that reported at lower temperatures, and it seems that the potential needed for 100% sulfate yield decreases with increasing temperature.

(3) The Ea for pyrite oxidation in 0.1 M sulfuric acid was obtained as 43.65, 68.67 and 63.19 kJ/mol, respectively at OCP, 200 and 400 mV vs. SHE, over the temperature range 160–240°C. Such values for the activation energy indicates that pyrite oxidation kinetics are limited by the rate of electrochemical reaction, and further demonstrates that temperature is a key factor for pyrite dissolution.

ORCID

Heping Li ◉ https://orcid.org/0000-0001-7814-0589

References

1. J. H. Hu, H. G. Huang, H. Z. Xie, L. H. Gan, J. Liu, and M. N. Long, *Biochem. Eng. J.*, **128**, 228 (2017).
2. T. T. Chen, L. J. Cabri, and J. E. Dutrizac, *J. Miner. Met. Mater. Soc.*, **54**, 20 (2002).
3. S. L. Mesa Espitia and G. T. Lapidus, *Hydrometallurgy*, **153**, 106 (2015).
4. Q. Y. Liu, M. Chen, and Y. Yang, *Electrochim. Acta*, **253**, 257 (2017).
5. P. Hazarika, B. Mishra, S. S. Chinnasamy, and H. J. Bernhardt, *Ore. Geol. Rev.*, **55**, 134 (2013).
6. A. Rabieh, B. Albijanic, and J. J. Eksteen, *Miner. Eng.*, **94**, 21 (2016).
7. V. A. Sundarrajan, Z. L. Li, Y. Z. Hu, X. H. Fu, and Y. H. Zhu, *Int. J. Earth Sci.*, **106**, 1057 (2017).
8. J. Li, B. Dabrowski, J. D. Miller, S. Acar, M. Dietrich, K. M. LeVier, and R. Y. Wan, *Miner. Eng.*, **19**, 883 (2006).
9. R. G. McDonald and D. M. Muir, *Hydrometallurgy*, **86**, 191 (2007).
10. M. Melashvili, C. Fleming, I. Dymov, D. Matthews, and D. Dreisinger, *Miner. Eng.*, **87**, 2 (2016).
11. H. R. Watling, *Hydrometallurgy*, **146**, 96 (2014).
12. C. A. Fleming, *Miner. Metall. Proc.*, **27**, 81 (2010).
13. I. V. Bylina, S. C. Mojumdar, and V. G. Papangelakis, *J. Therm. Anal. Calorim.*, **108**, 829 (2012).
14. K. Tozawa and K. Sasaki, *Cim Bull.*, **79**, 107 (1986).
15. G. L. Hu, K. Dam-Johansen, W. Stig, and J. P. Hansen, *Prog. Energ. Combust.*, **32**, 295 (2006).
16. L. Rusanen, J. Aromaa, and O. Forsen, *Physicochem. Probl. Mi.*, **49**, 101 (2013).
17. A. Gartman and G. W. Luther, *Geochim. Cosmochim. Ac.*, **144**, 96 (2014).
18. Z. H. Tu, J. J. Wan, C. L. Guo, C. Fan, T. Zhang, G. N. Lu, J. R. Reinfelder, and Z. Dang, *Electrochim. Acta*, **239**, 25 (2017).
19. Q. Y. Liu and H. P. Li, *Miner. Eng.*, **23**, 691 (2010).
20. D. R. Mckay and J. Halpern, *Trans. Metall. Soc. AIME*, **212**, 301 (1958).
21. A. P. Chandra and A. R. Gerson, *Surf. Sci. Rep.*, **65**, 293 (2010).
22. W. E. King Jr. and J. A. Lewis, *Ind. Eng. Chem. Proc. Des. Dev.*, **19**, 719 (1980).
23. L. K. Bailey and E. Peters, *Can. Metall. Quart.*, **15**, 333 (1976).
24. V. G. Papangelakis and G. P. Demopoulos, *Hydrometallurgy*, **26**, 309 (1991).
25. H. Long and D. G. Dixon, *Hydrometallurgy*, **73**, 335 (2004).
26. V. V. Zhukov, A. Laari, and T. Koiranen, *Ind. Eng. Chem. Res.*, **54**, 9920 (2015).
27. F. P. Gudyanga, T. Mahlangu, R. J. Roman, J. Mungoshi, and K. Mbeve, *Miner. Eng.*, **12**, 863 (1999).
28. G. H. Qiu, T. Y. Gao, J. Hong, W. F. Tan, F. Liu, and L. R. Zheng, *Geochim. Cosmochim. Ac.*, **217**, 306 (2017).
29. R. Zarate-Gutierrez, G. T. Lapidus, and R. D. Morales, *Hydrometallurgy*, **115**, 57 (2012).
30. M. M. McGuire, K. N. Jallad, D. Ben-Amotz, and R. J. Hamers, *Appl. Surf. Sci.*, **178**, 105 (2001).
31. J. L. Xia, Y. Yang, H. He, X. J. Zhao, C. L. Liang, L. Zheng, C. Y. Ma, Y. D. Zhao, Z. Y. Nie, and G. Z. Qiu, *Hydrometallurgy*, **100**, 129 (2010).
32. Z. H. Tu, C. L. Guo, T. Zhang, G. N. Lu, J. J. Wang, C. J. Liao, and Z. Dang, *Hydrometallurgy*, **167**, 58 (2017).
33. M. N. Lehmann, M. Stichnoth, D. Walton, and S. I. Bailey, *J. Electrochem. Soc.*, **147**, 3263 (2000).
34. G. Urbano, V. E. Reyes, M. A. Veloz, I. Gonzalez, and J. Cruz, *J. Phys. Chem. C*, **112**, 10453 (2008).
35. B. Guo, Y. J. Peng, and G. Parker, *Miner. Eng.*, **92**, 78 (2016).
36. D. D. Macdonald, A. C. Scott, and P. Wentrcek, *J. Electrochem. Soc.*, **126**, 1618 (1979).
37. E. Huttunen-Saarivirta, P. Rajala, M. Bomberg, and L. Carpen, *Electrochim. Acta*, **240**, 163 (2017).
38. J. Li, L. Ecco, G. Delmas, N. Whitehouse, P. Collins, F. Deflorian, and J. S. Pan, *J. Electrochem. Soc.*, **162**, C55 (2015).
39. P. Cordoba, T. J. Mesquita, O. Devos, B. Tribollet, V. Roche, and R. P. Nogueira, *Electrochim. Acta*, **72**, 172 (2012).
40. A. Ghahremaninezhad, D. G. Dixon, and E. Asselin, *Hydrometallurgy*, **125**, 42 (2012).
41. T. Nagai and H. Kiuchi, *Nippon Kogyo Kaishi*, **91**, 547 (1975).
42. J. R. Flatt and R. Woods, *J. Appl. Electrochem.*, **9**, 852 (1995).
43. E. Ahlberg and A. E. Broo, *J. Electrochem. Soc.*, **144**, 1281 (1997).
44. W. Qin, X. Wang, L. Ma, F. Jiao, R. Liu, C. Yang, and K. Gao, *Miner. Eng.*, **74**, 99 (2015).
45. R. Murphy and D. R. Strongin, *Surf. Sci. Rep.*, **64**, 1 (2009).
46. W. Zhao, H. Zhu, Z. M. Zong, J. H. Xia, and X. Y. Wei, *Fuel*, **84**(2-3), 235 (2005).
47. S. N. Esmaeely and S. Nesic, *J. Electroanal. Chem.*, **12**, C664 (2017).
48. F. Zipoli, R. Car, M. H. Cohen, and A. Selloni, *J. Am. Chem. Soc.*, **25**, 8593 (2010).
49. W. Liu, E. Y. Hu, H. Jiang, Y. J. Xiang, Z. Weng, M. Li, Q. Fan, X. Q. Yu, E. Altman, and H. L. Wang, *Nat. Commun.*, **7**, 10771 (2016).
50. A. S. Quist, W. L. Marshall, and H. R. Jolley, *J. Phys. Chem.*, **8**, 2726 (1965).
51. P. R. Holmes and F. K. Crundwell, *Geochim. Cosmochim. Ac.*, **2**, 263 (2000).
52. I. C. Hamilton and R. Woods, *J. Electroanal. Chem.*, **118**, 327 (1981).
53. T. Biegler and D. A. Swift, *Electrochim. Acta*, **24**, 415 (1979).